Bromide Electrosorption on Liquid Gallium: A Typical Example of Halide Electrosorption from Aqueous Solutions and Its Modeling†

Giovanni Pezzatini, Massimo Innocenti, Maria Luisa Foresti, and Rolando Guidelli*

Dipartimento di Chimica, Universita' di Firenze, Via G. Capponi 9, 50121 Firenze, Italy

Received: August 13, 1996; In Final Form: November 29, 1996⊗

The adsorption of bromide ion on liquid gallium from aqueous solutions of NaBr + HBr of concentrations ranging from 0.02 to 1.99 M was determined on the basis of capacitive charge measurements carried out by a computerized chronocoulometric technique. This adsorption is parametrized by the use of the virial isotherm corrected for the potential difference across the diffuse layer. The resulting adsorption behavior has several features in common with chloride, bromide, and iodide adsorption on mercury. These general features are interpreted on the basis of a molecular model that accounts for the local potential at the position of an adsorbed anion created by the surrounding anions as well as by the water dipoles. The fundamental role played by the mutual interactions among the adsorbed anions, the adsorbed water dipoles, and the inhomogeneous electron gas, the latter treated on the basis of a simple one-parameter jellium model, is pointed out.

Introduction

Ionic adsorption on mercury from aqueous solutions has been examined very thoroughly,[1−12] and interpretations based on models accounting for discreteness-of-charge effects have been provided.[13−25] Despite the pioneering work by Frumkin, Bagotskaya, et al.[26−32] aiming at extending adsorption measurements from mercury to liquid gallium, there are very few papers concerning ionic adsorption on this metal. The main reason for this is the narrow potential range within which this metal is electroinactive. Other reasons relate to the experimental difficulties associated with the handling of Ga. On the other hand, Ga is the only pure metal, beside Hg, that is liquid near room temperature and that, as such, allows a number of complications inherent in the use of solid metals to be avoided. Moreover, Ga and Hg differ notably in one of the main distinguishing feature of metals, namely, hydrophilicity.[33,34] Hence, there remains a continuing interest in comparative adsorption studies on Hg and Ga.[35−46]

In the early work of the Russian school the adsorption on Ga of several anions, including bromide, was evaluated from interfacial tension or differential capacity measurements.[26−28,32] Only surface excesses $\Gamma_{-,w}$ relative to water were reported. No attempt was made to correct these thermodynamic excesses for the diffuse layer contribution in order to obtain the specifically adsorbed surface excesses Γ^{i}_{-}, since at that time it was believed that the Gouy−Chapman theory for the diffuse layer did not apply to the Ga electrode.[29] This pioneering work suffers sometimes from inaccuracy due to the later recognized strong influence of the purity of the metal and the intrinsic lack of precision in measuring the potential of zero charge;[37,40,45] anyhow, it established many interesting semiquantitative correlations among the adsorptivities of different anions on Ga as well as between the adsorptivities of each anion on Ga and on Hg.

Subsequently, a special dropping gallium electrode set up in our laboratory,[36] used in combination with a computerized chronocoulometric technique for capacitive charge measurements,[36,39] permitted us to achieve more accurate results. It was therefore possible to verify the validity of the Gouy−Chapman theory at the interface between liquid Ga and aqueous solutions of the nonspecifically adsorbed $NaClO_4$[40] and Na_2SO_4[45] salts. A slight specific adsorption of the perchlorate anion on Ga was only observed at $NaClO_4$ concentrations higher than 1 M.[40]

The present work deals with the electrosorption of bromide ion on Ga from its pure salt KBr and represents the first thorough investigation of the specific adsorption of an anion on Ga, based on a thermodynamic analysis of capacitive charge measurements and on the Grahame−Soderberg[47] procedure. The resulting adsorption isotherms at constant charge density σ_M exhibit a number of features common to those reported for the adsorption of halide ions on mercury. These features will be interpreted on the basis of a molecular model of ionic specific adsorption that accounts for the screening effect exerted on the adsorbed anions by the surrounding water dipoles as well as by the inhomogeneous electron gas.

Experimental Section

Merck suprapur NaBr and HBr were used without further purification. The water used was obtained from light mineral water by distilling it once and by then distilling the water so obtained from alkaline permanganate while constantly discarding the heads. Johnson Matthey & Co. gallium of 99.9999% purity was employed.

The dropping gallium electrode consisted of a glass reservoir joined to a capillary made up of polyethylene to avoid sticking and was employed as described in ref 36, with a few further improvements reported in ref 39. Chronocoulometric measurements were carried out with a computerized apparatus making use of a Model DG10 microcomputer from Data General. Absolute charge values were obtained by correcting the charge flowing into a potentiostated dropping gallium electrode for the faradaic contribution,[39] whereas changes $\Delta\sigma_M$ of capacitive charge density in passing from an initial to a final potential were obtained by integrating the current following the corresponding potential step.[36,39] All potentials are referred to the saturated calomel electrode (SCE). All measurements were carried out at 32 ± 0.1 °C.

The double-layer region at a gallium/water interface shifts toward less negative potentials and becomes narrower with a progressive decrease in pH. To cover the largest possible

† Presented at the International Workshop on "Electrochemistry, Solid vs Liquid State", Schloss Ringberg, Tegernsee, Germany, March 4−8, 1996.

⊗ Abstract published in *Advance ACS Abstracts,* March 1, 1997.

S1089-5647(96)02443-1 CCC: $14.00

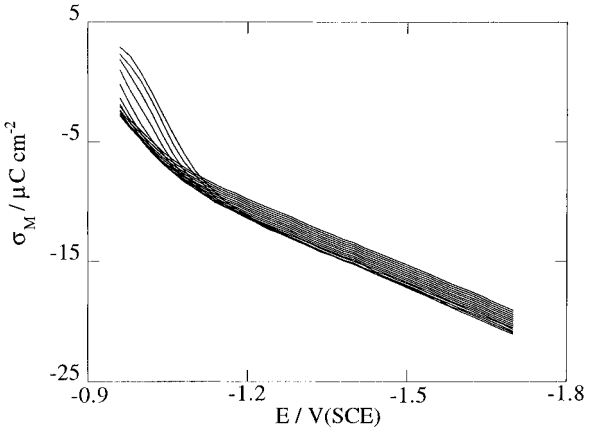

Figure 1. Plots of σ_M vs E for NaBr + HBr adsorption on Ga at bromide concentrations varying from 2.24×10^{-2} to 1.99 M by 0.15 logarithmic increments when proceeding downward on the right-hand side of the figure.

potential range, the pH of x M HBr + $(c - x)$ M NaBr solutions, of overall bromide concentration c, was progressively decreased by steps small enough as to obtain an overlapping of the $\Delta\sigma_M$ vs E curves relative to contiguous pH values over a potential range of no less than 60 mV. By the above procedure $\Delta\sigma_M$ vs E curves at each bromide concentration c were constructed over the potential range from −1.0 to −1.7 V/SCE. Bromide ion activities for $c > 0.2$ M were taken as equal to the mean ionic activities of pure NaBr as obtained by interpolation of tabulated values.[48] The mean ionic activity coefficients for $c < 0.2$ M were calculated from Davies' formula.[49] The change in the activity coefficient following the substitution of Na^+ with H^+ was constantly disregarded; incidentally, at the lowest c value employed the maximum value of x was about $0.3c$.

Results

Figure 1 shows experimental curves of $\sigma_M(E,c)$ vs E as obtained upon varying the bromide concentration, c, by 0.15 logarithmic increments from 2.24×10^{-2} to 1.99 M.

The specific adsorption of bromide ion was determined by the same procedure adopted for perchlorate adsorption,[40] with some minor modifications. Thus, the relative surface excess $\Gamma_{+,w}(\sigma_M,c)$ of cations was obtained from the thermodynamic relationship

$$\Gamma_{+,w}(\sigma_M,c) = \Gamma_{+,w}(\sigma_{M,n},c) - \frac{1}{2RT}\int_{\sigma_{M,n}}^{\sigma_M}\left(\frac{\partial E_-}{\partial \ln a_\pm}\right)_{\sigma_M} d\sigma_M \qquad (1)$$

Here $\sigma_{M,n} = -19\ \mu$C cm^{-2} is the most negative charge density that is experimentally accessible and at which bromide specific adsorption can be legitimately ruled out, $E_- \approx E + (RT/F) \ln a_\pm$ is the potential measured relative to a reference electrode reversible to the anion, and $a_\pm$ is the mean ionic activity. The $\Gamma_{+,w}(\sigma_{M,n},c)$ value in eq 1 was estimated from the Gouy−Chapman expression for the cationic surface excess in the diffuse layer.

Figure 2 shows plots of $\sigma_{+,w}(\sigma_M,c) \equiv F\Gamma_{+,w}(\sigma_M,c)$ vs σ_M for the 14 concentrations employed. At far negative potentials they practically coincide with the corresponding plots for $NaClO_4$ electrosorption on Ga,[40] but they start to deviate from the unit slope expected for nonspecifically adsorbed electrolytes at lower concentrations and at more negative σ_M values. This indicates that bromide is much more strongly adsorbed than perchlorate on Ga, in agreement with the conclusions by Morozov et al.[27] The plots in Figure 2 are confined to σ_M values negative to −3 μC cm^{-2}, where accurate mesurements could be carried out over

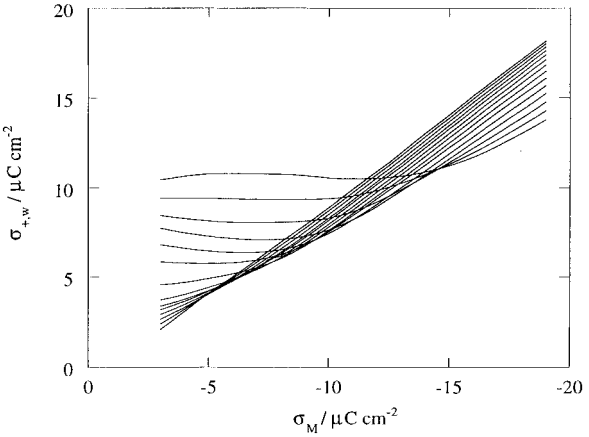

Figure 2. Plots of $\sigma_{+,w}$ vs σ_M for NaBr + HBr adsorption on Ga at the same bromide concentrations as in Figure 1.

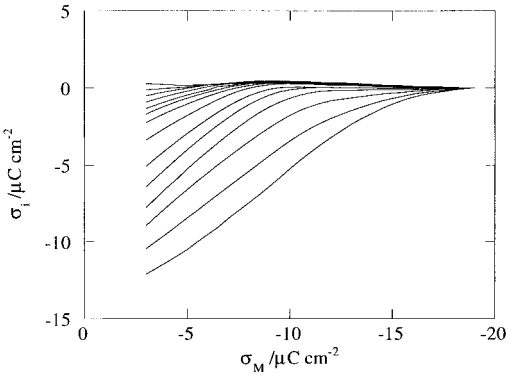

Figure 3. Plots of σ_i vs σ_M for NaBr + HBr adsorption on Ga at the same bromide concentrations as in Figure 1.

the whole concentration range investigated. After identifying $\Gamma_{+,w}(\sigma_M,c)$ with the corresponding cationic surface excess in the diffuse layer, $\Gamma^d_+(\sigma_M,c)$, the corresponding bromide surface excess in the diffuse layer, $\Gamma^d_-(\sigma_M,c)$, was derived by the Grahame−Soderberg procedure[47] and the surface excess $\Gamma^i_-(\sigma_M,c)$ due to the specifically adsorbed bromide ions was finally obtained from the equation

$$\Gamma^i_-(\sigma_M,c) = \frac{\sigma_M}{F} + \Gamma^d_+(\sigma_M,c) - \Gamma^d_-(\sigma_M,c)$$

Figure 3 shows plots of $\sigma_i \equiv -F\Gamma^i_-$ vs σ_M at the different concentrations investigated. The usual concentration dependence of adsorption, typical of all simple ionic systems on mercury, is displayed. The limiting slope $(-d\sigma_i/d\sigma_M)$ of these plots is 1.1. This value may be compared with the limiting slope, 1.35, of the corresponding plot for 0.1 M KBr on Hg.[11] Figure 4 shows plots of σ_i vs $(RT/F) \ln a_\pm$ at constant σ_M, namely, the adsorption isotherms. The dashed curves are the isotherms for bromide adsorption from aqueous KBr on Hg relative to three different σ_M values, as taken from ref 9. By comparing the isotherms on Ga and Hg at the same σ_M value it is apparent that at the lower mean ionic activities bromide adsorption is lower on Ga than on Hg, whereas the opposite is true at the higher activities: on the average, bromide adsorptivity on Ga is comparable with that on Hg. These results do not support the conclusions by Morozov et al.,[27] according to which bromide is less strongly adsorbed on Ga than on Hg.

By subtracting the potential difference ϕ_d across the diffuse layer from the applied potential E we obtain the potential difference ϕ^{M-2} across the inner layer, apart from an additive constant. Figure 5 shows plots of $E - \phi_d$ vs σ_i at different

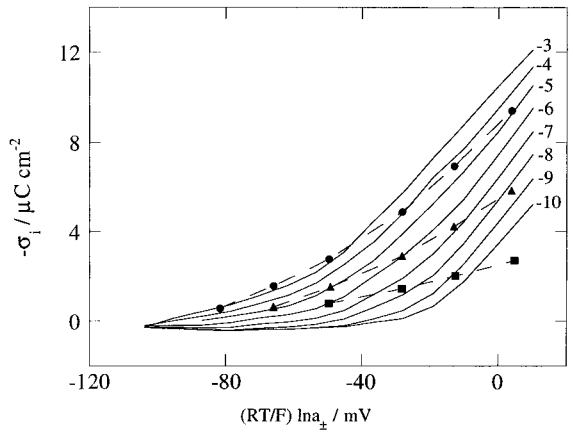

Figure 4. Plots of $-\sigma_i$ vs (RT/F) ln $a_\pm$ for NaBr + HBr adsorption on Ga at different charge densities on the metal (solid curves). Numbers on each curve denote σ_M values in μC cm^{-2}. The dashed curves are corresponding curves for KBr adsorption on mercury at $\sigma_M = -4$ (●), -6 (▲), and -8 μC cm^{-2} (■), as derived from Figure 6 in ref 7.

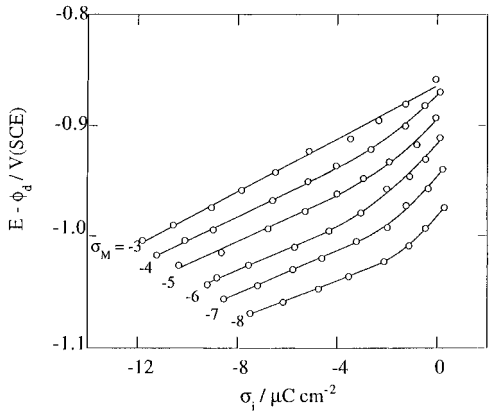

Figure 5. Plots of $E - \phi_d$ vs σ_i for NaBr + HBr adsorption on Ga at different σ_M values. Numbers on each curve denote σ_M values in μC cm^{-2}.

charge densities σ_M. These plots are linear at the higher $|\sigma_i|$ values, but exhibit a slight curvature at the lower values. Similar deviations from linear behavior were observed for chloride,[2] bromide,[7] and azide[10] adsorption on mercury. Extrapolation of the linear portion of each of these plots until it intersects the vertical straight line corresponding to a σ_i value equal and opposite to the corresponding σ_M value yields a roughly linear plot of E vs σ_i for a "grounded" electrode, i.e. an electrode that is characterized by $\sigma_i = -\sigma_M$ and hence by the absence of the diffuse layer. The slope of the latter plot, 1.9×10^{-2} cm^2 μF^{-1}, is a measure of the dipole moment created by an adsorbed bromide ion and by its image in the metal surface plane.[50−52] In the present case this dipole moment is about equal to -0.8 D and hence is comparable with that on mercury (-0.95 D),[52] but somewhat higher than those on Ag(111) (-0.23 D) and on Ag(100) (-0.31 D).[53] The common slope of the linear portions of the $E - \phi_d$ vs σ_i plots in Figure 5 measures the reciprocal of the inner layer capacity ${}_{\sigma i}C_i = (\partial\sigma_i/\partial\phi^{M-2})_{\sigma M}$ at constant σ_M, whereas the separation of these linear portions along the vertical axis yields the reciprocal of the inner layer capacity ${}_{\sigma M}C_i = (\partial\sigma_M/\partial\phi^{M-2})_{\sigma i}$ at constant amount adsorbed. The ratio of these two capacities, ${}_{\sigma M}C_i/{}_{\sigma i}C_i$, which in the present case amounts to $(\sim 40\ \mu\text{F cm}^{-2})/(\sim 90\ \mu\text{F cm}^{-2}) = 0.44$, was sometimes regarded as a measure of the "thickness ratio" $(d - \beta)/d$,[3] where d is the thickness of the inner layer and β is the distance of the locus of the charge centers of the specifically adsorbed anions from the metal surface. Nowdays, this modelistic interpretation of this capacity ratio is usually regarded as questionable,[8,54] in view of the very crude model on which it relies.

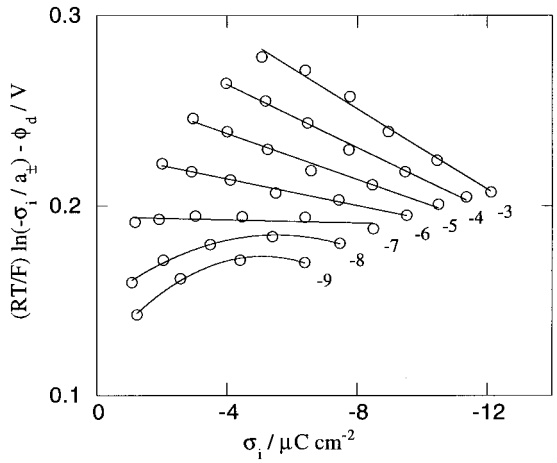

Figure 6. Plots of (RT/F) ln $(-\sigma_i/a_\pm) - \phi_d$ vs σ_i for NaBr + HBr adsorption on Ga at different charge densities on the metal. Numbers on each curve denote σ_M values in μC cm^{-2}.

Discussion

The adsorption isotherms in Figure 4 can be compared with the prediction of the virial isotherm corrected for ϕ_d:[10,11,55]

$$\ln(-\sigma_i) = \ln a_\pm + \frac{(-\Delta G^\circ + 2B\sigma_i + F\phi_d)}{RT} \qquad (2)$$

where ΔG° is the standard Gibbs energy of adsorption, B is a second-virial coefficient, and the term in ϕ_d arises from the contribution to the adsorption energy of the ion due to its transfer across the diffuse layer. The use of an isotherm such as this, which neglects the attainment of saturation, is entirely justified in the present case. Thus, the maximum charge density σ_i attained in our measurements (~ 12 μC cm^{-2}) is less than one-tenth of the saturation value (133 μC cm^{-2}) calculated for a hexagonally packed array of spheres of radius 1.95 Å. According to eq 2 a plot of $\ln(-\sigma_i/a_\pm) - F\phi_d/RT$ vs σ_i at constant σ_M should be linear, with an intercept equal to $-\Delta G^\circ/(RT)$ and a slope equal to $2B/(RT)$. If the slope is independent of σ_M, then the dependence of the isotherm on this electrical variable is completely contained in ΔG°. In this case solute−solute interactions and solute−metal interactions act independently of each other, the former being accounted for by B and the latter by ΔG°. Nowdays, a large amount of experimental evidence and straightforward theoretical considerations[56] exclude the fulfillment of the above expectations. This is because the correlations between adsorbed solute molecules are transmitted not only directly but also indirectly, via the solvent molecules populating the interface and the inhomogeneous electron gas, both affected by the electrical variable. Nonetheless, a fitting of experimental isotherms to the corrected virial isotherm is still useful, because it serves to verify the extent of the deviations from a complete independence of solute−solute and solute−metal interactions.

Even though the (RT/F) ln $(-\sigma_i/a_\pm) - \phi_d$ vs σ_i plots in Figure 6 are satisfactorily linear only for $\sigma_M > -8$ μC cm^{-2}, it is apparent that their slope decreases rapidly as σ_M becomes progressively more negative and ultimately becomes slightly negative: this indicates strong interconnections between solute−solute and solute−metal interactions. The dependence of both B and ΔG° upon σ_M is shown in Figure 7; here B is in nm^2/molecule and ΔG° refers to a standard state of unit molarity in solution and 1 ion cm^{-2} on the metal surface. The standard

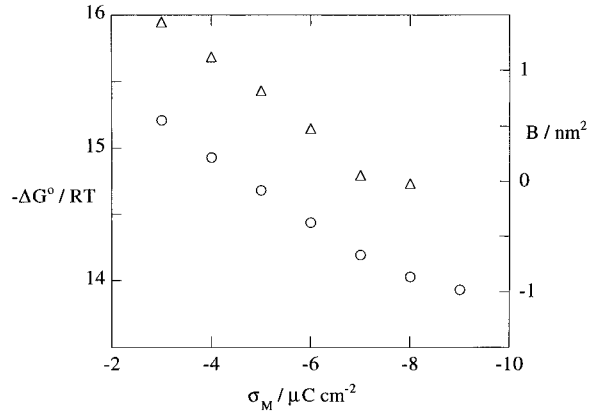

Figure 7. Plots of $-\Delta G°/(RT)$ (○) and of B (△) vs σ_M for NaBr + HBr adsorption on Ga.

free energy of adsorption $\Delta G°$ decreases linearly with an increase in σ_M, a behavior shared by the adsorption of halide ions on mercury[11] and often explained on the basis of simple models that embody in $\Delta G°$ the whole dependence of the isotherm on σ_M. As a matter of fact, the linear dependence of $\Delta G°$ on σ_M by no means implies the congruence of the corresponding isotherm with respect to charge, an unsupported expectation which is disproved by the charge dependence of the second-virial coefficient. A progressive decrease in the slope of $(RT/F)\ln(-\sigma_i/a_\pm) - \phi_d$ vs σ_i plots at constant σ_M with a negative shift in σ_M, accompanied by a slight downward curvature of these plots, is also observed in the adsorption of chloride,[8] bromide,[7] and iodide[1] on mercury (see Figure 8). This decrease in slope is more pronounced the lower the adsorptivity of the anion, namely, in passing from iodide to chloride. It is interesting to compare the charge dependence of $\Delta G°$ and B for bromide adsorption on Ga and Hg, as obtained from the intercepts and slopes of the linear portions of the corrected virial isotherms in Figures 6 and 8. From Figure 9 it is apparent that the $\Delta G°$ vs σ_M plots on Hg and Ga lie roughly on the same straight line, thus confirming that the adsorptivity of bromide ion is practically the same on these two metals, once due account is taken of its charge dependence. The charge dependence of the second-virial coefficient B also shows the same trend on Hg and Ga, although the decrease in B with a negative shift in σ_M is more rapid on Ga than on Hg.

The above general features of halide adsorption on Hg and Ga, with particular regard to the deviations from the predictions of a corrected virial isotherm assuming an independence of solute−solute and solute−metal interactions, will be examined in the light of a molecular model of ionic adsorption.

The Adsorption Isotherm. A justification for the use of a "corrected" virial isotherm stems from the consideration that at equilibrium the electrochemical potential $\tilde{\mu}^{b}_{i}$ of a monovalent anion in the bulk solution is equal to that, $\tilde{\mu}^{ads}_{i}$, in the adsorbed state:

$$\tilde{\mu}^{b}_{i} = \mu^{0,b}_{i} + kT\ln c_i = \tilde{\mu}^{ads}_{i} = \mu^{0,ads}_{i} + kT\ln(-\sigma_i) + \int_0^{-e}\phi_{loc}(q)\,dq \quad (3)$$

Here $\mu^{0,b}_{i}$ and $\mu^{0,ads}_{i}$ are standard chemical potentials in the bulk and in the adsorbed state respectively, and c_i is the anion concentration in the bulk solution, whereas the corresponding surface concentration is expressed by the charge density σ_i of the specifically adsorbed anions. The electrical term consists of the "local potential" ϕ_{loc} at the position of an adsorbed anion, with the anion fixed and the surrounding particles statistically distributed around it.[16] The charge q of the monovalent anion must be increased gradually from 0 to its maximum value $-e$ according to the Guntelberg charging process: hence, it is the

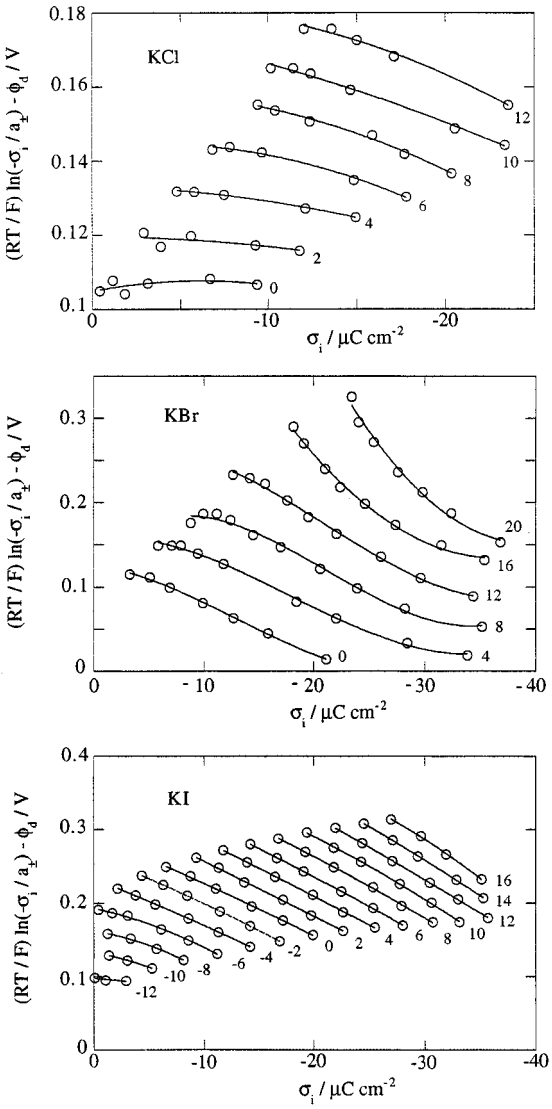

Figure 8. Plots of $(RT/F)\ln(-\sigma_i/a_\pm) - \phi_d$ vs σ_i for the adsorption of KCl, KBr, and KI at different charge densities on the metal, as reported in Figures 11D, 12D, and 13D of ref 11. The original data for KCl, KBr, and KI adsorption were taken from refs 8, 7, and 1. Numbers on each curve denote σ_M values in μC cm^{-2}.

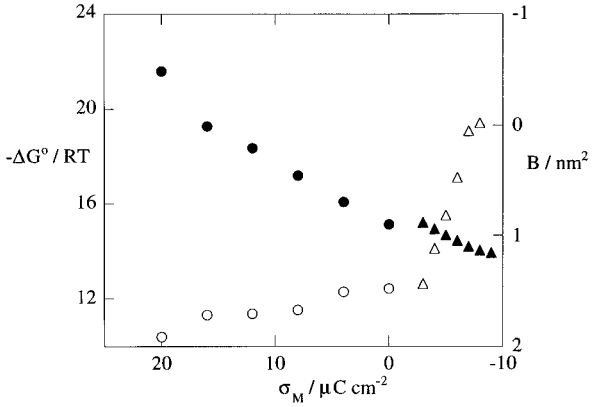

Figure 9. $\Delta G°/(RT)$ vs σ_M plots for NaBr + HBr adsorption on Ga (▲) and for KBr adsorption on Hg (●); B vs σ_M plots for NaBr + HBr adsorption on Ga (△) and for KBr adsorption on Hg (○). The data on Hg were obtained by least squares fitting to a straight line of the intermediate linear portion of the $(RT/F)\ln(-\sigma_i/a_\pm) - \phi_d$ vs σ_i plots for KBr adsorption in Figure 8.

mean value of the local potential ϕ_{loc} during this charging process that must be estimated. The local potential relative to the bulk solution can be regarded as the sum of the corresponding "mean potential", namely, the potential at a point with no ion permanently located at that point, and of a "perturbation" (or "fluctuation") potential ϕ_p, which measures the deviation of the local potential from its mean value.

Let us denote by $x = \beta$ the locus of the centers of charge of the adsorbed anions (the inner Helmholtz plane, iHp) and by $x = d$ the outer boundary of the adsorbed monolayer (the outer Helmholtz plane, oHp), both measured relative to the electrode surface plane, $x = 0$. The mean potential can then be expressed as the sum of the mean potential difference $\phi^{\beta-d}$ between β and d plus the potential difference ϕ_d across the diffuse layer, which can be approximately estimated on the basis of the Gouy−Chapman theory. Rearranging terms, eq 3 can be written

$$\frac{kT}{e}\ln\left(\frac{-\sigma_i}{c_i}\right) - \phi_d = \text{const} + \phi^{\beta-d} - \frac{1}{e}\int_0^{-e}\phi_p(q)\,dq \quad (4)$$

where the left-hand side can be plotted against σ_i at a constant charge density σ_M on the metal. The experimental behavior of this plot is to be compared with the behavior of the mean value of the local potential during the charging process, with the obvious exclusion of contribution from ϕ_d. While a positive slope of the above plots is suggestive of a repulsion between the adsorbed anions, a negative one is apparently suggestive of an attraction. It is evident that a screening of the charged ions, no matter how large, cannot account for an apparent attractive interaction unless the screening increases with an increase in the surface concentration of the ions.

The Model. To account for the above behavior, we shall assume that the adsorbed bromide ions are arranged in the two-dimensional structure that minimizes their interaction energy, i.e. a hexagonal array. The nearest neighbor distance for this array is $s = (43.011/\sqrt{\sigma_i})$ Å, when the charge density σ_i of the bromide ions is expressed in μC cm^{-2}. The adsorbed monolayer consisting of water molecules and bromide ions is enclosed between the electrode surface plane $x = 0$ and the oHp, $x = d$. The water molecules are simulated by spheres of radius $r_w = 1.5$ Å, with an embedded point dipole of permanent dipole moment $\mu_w = 1.82$ D; the bromide ions are simulated by spheres of radius $r_{Br} = 1.95$ Å, with a point charge $-e$ in their center. The distortional polarization of the water molecules is accounted for by the use of a distortional dielectric constant, although the concept of a dielectric constant as applied to a monolayer is not neatly definable. In monolayer models, the distortional dielectric constant $\epsilon_\uparrow$ used in expressing the mean potential difference across the monolayer is normally ascribed to values close to 6, in order to match the experimental differential capacity at metal/water interfaces for high $|\sigma_M|$ values.[57] This relatively high value stems from a limitation of all monolayer models, namely, the lack of direct correlations between the water molecules in the monolayer and those in the bulk solution phase. Hydrogen bond formation between the adsorbed water molecules and the overhanging water molecules of the contacting solution phase tends to oppose full alignment of the adsorbed molecules under the effect of the external electric field $4\pi\sigma_M$: the relatively high value ascribed to $\epsilon_\uparrow$ produces roughly the same effect. A different distortional dielectric constant, $\epsilon_\rightarrow$, should be employed to account for the effect of water polarizability upon the interaction energy between adsorbed ions. This is because the local electric fields created by these ions vary rapidly in magnitude and direction over the dimensions characterizing the microscopic structure of the monolayer; this prevents strong direct correlations between the adsorbed water molecules. Thus, Barlow and Macdonald[15] consider the dielectric constant parallel to the monolayer to be on the order of unity. A rough estimate of $\epsilon_\rightarrow$ can be made by setting it equal to its mean-field value for a monolayer, $(1 + \alpha_w b/d^3)$,[58] where α_w is the scalar polarizability of water, b is a lattice sum that equals 11.034 for a hexagonal lattice and d is the monolayer thickness. If a water molecule is approximated to a conducting sphere of radius $r_w = 1.5$ Å, then its scalar polarizability is given by $r_w^3 = 3.38$ Å^3; for $d = 3$ Å, $\epsilon_\rightarrow$ amounts to 2.4.

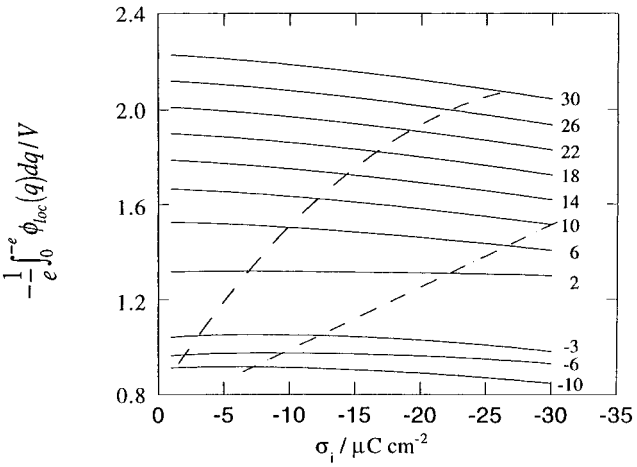

Figure 10. Plots of $-(1/e)\int_0^{-e}\phi_{loc}(q)\,dq$ against σ_i as calculated from eqs A6−A10 for $\beta = 1.5$ Å, $d = 3$ Å, $\epsilon_\uparrow = 6$, $\epsilon_\rightarrow = 2.6$, and $n = 0.0234$ au. Numbers on each curve denote σ_M values.

The inhomogenous electron gas is treated on the basis of a simple one-parameter jellium model making use of the Partenskii−Smorodinskii trial function.[59] The point charges and dipoles within the monolayer are imaged an infinite number of times (C−C imaging[15] at $x = d$ on the solution side and at the "image plane" x_{im}, as estimated from the jellium model, on the metal side. The progressive outward shift of the image plane with a negative shift in the charge density σ_M accounts for the concomitant increase in the screening of the charges and dipoles by the electron gas. The treatment of this model is outlined in the Appendix.

Conclusions

The mean value $-(1/e)\int_0^{-e}\phi_{loc}(q)\,dq$ of the overall local potential ϕ_{loc} resulting from the sum of the potential due to the inhomogeneous electron gas (eq A6), the local potential due to the surrounding ions (eqs A7 and A8), and the local potential due to the surrounding water dipoles (eqs A9 and A10) is plotted in Figure10 as a function of σ_i at different charge densities σ_M on the metal; the calculations were carried out setting $\beta = 1.5$ Å, $d = 3$ Å, $\epsilon_\uparrow = 6$, $\epsilon_\rightarrow = 2.6$, and the bulk electron density n equal to its value for Ga, 0.0234 au. The behavior of these calculated plots is to be compared with that of experimental plots of $(RT/F)\ln(-\sigma_i/a_\pm) - \phi_d$ vs σ_i. It can be seen that the calculated plots are slightly curved, with a downward concavity. In addition, over the range of σ_i values that is experimentally accessible and is approximately enclosed between the two dashed lines in the figure, they exhibit a positive slope whose absolute value decreases gradually as σ_M becomes progressively more negative. Ultimately, at sufficiently negative σ_M values, the slope may even become slightly negative. All these features account for the adsorption behavior of halide ions. Even though the values of the calculated slopes depend somewhat on the parameters of the adsorbed monolayer, for all reasonable values of these parameters these features are retained.

The reason for the decrease in the positive value of the slope is to be found in the interplay between electron spillover and the orientation of the water dipoles. At negative charge densities on the metal and in the absence of adsorbed anions the water dipoles are partially oriented with their positive end toward the metal: hence, the potential difference created by these dipoles tends to oppose the electron spillover. The gradual reorientation of these water dipoles parallel to the electrode surface plane with an increase in $|\sigma_i|$ progressively removes this opposition, causing an increase in the extent of the electron spillover; the resulting outward shift of the image plane causes an increase in the screening effect of the electron gas. It follows that an increase in the surface concentration of the adsorbed anions is accompanied by a shift in the local potential that is only slightly negative, and that may even become positive at sufficiently negative σ_M values, when the water dipoles are strongly oriented by the external field in the absence of adsorbed anions. An opposite situation is encountered at positive charge densities on the metal, when the water dipoles in the absence of adsorbed anions are oriented with the negative end toward the metal and hence originate a potential difference that favors electron spillover. In this case, a gradual increase in the surface concentration of the adsorbed anions, by causing both a reorientation and a removal of the adsorbed water dipoles, decreases the extent of electron spillover and hence its screening effect. This produces a more rapid negative shift of the local potential ϕ_{loc} with an increase in $|\sigma_i|$. Ultimately, at sufficiently positive σ_M values, the slope of the $-(1/e)\int_0^{-e}\phi_{loc}(q)\,dq$ vs σ_i plot attains a limiting positive value because the interaction between electron spillover and adsorbed water dipoles becomes negligibly small even in the absence of adsorbed bromide ions.

Appendix

The Mean Vertical Electric Field. Before estimating the local potential ϕ_{loc}, it is convenient to calculate the mean vertical electric field $\bar{F}_\uparrow$ acting on the water molecules. The contribution to $\bar{F}_\uparrow$ from the free charges (i.e. the jellium, the electron gas, and the bromide ions) is obtained by noting that the corresponding volume charge density $\rho(x)$ as a function of the distance x from the electrode surface plane is given by

$$\rho(x) = \begin{cases} (n^* + \alpha\sigma_M)e^{\alpha x}/2 & \text{for } x < 0 \\ -(n^* - \alpha\sigma_M)e^{-\alpha x}/2 + \delta(\beta - x)\sigma_i & \text{for } x > 0 \end{cases} \quad \text{(A1)}$$

Here n^* is the electron density in the bulk metal, α is the variational parameter in the Partenskii−Smorodinskii trial function,[59] and δ is the Dirac delta function. On substituting $\rho(x)$ in the Poisson differential equation of electrostatics and integrating once over x between the bulk metal ($x = -\infty$), of dielectric constant $\epsilon = 1$, and a point $x > 0$ within the adsorbed monolayer, with a distortional dielectric constant $\epsilon_\uparrow$, we obtain the following expression for the vertical electric field $F_\uparrow$ due to the free charges:

$$F_\uparrow = \begin{cases} 2\pi\left(\frac{n^*}{\alpha} + \sigma_M\right)e^{\alpha x} & \text{for } x < 0 \\ \frac{4\pi\sigma_M}{\epsilon_\uparrow} + \frac{2\pi}{\epsilon_\uparrow}\left(\frac{n^*}{\alpha} - \sigma_M\right)e^{-\alpha x} & \text{for } 0 < x < \beta \\ \frac{4\pi\sigma_M}{\epsilon_\uparrow} + \frac{2\pi}{\epsilon_\uparrow}\left(\frac{n^*}{\alpha} - \sigma_M\right)e^{-\alpha x} + \frac{4\pi\sigma_i}{\epsilon_\uparrow} & \text{for } x > \beta \end{cases} \quad \text{(A2)}$$

The single variational parameter α is obtained by minimizing the surface energy functional $E(n)$. Explicit expressions for the kinetic, exchange, and correlation energies of the inhomogeneous electron gas and for the gradient expansion term of the kinetic energy are given by Smith.[60] The electrostatic contribution to $E(n)$ required to assemble the free charges of the interface and to bring the water molecules into the field of this charge distribution is given by[61]

$$E_{es} = \frac{1}{8\pi}\int_{-\infty}^{d} F_\uparrow^2\,dx - \frac{1}{2}\int_0^d PF_\uparrow\,dx \quad \text{with} \quad P \equiv \frac{\langle\mu_\uparrow\rangle N_w}{d} \quad \text{(A3)}$$

Here $F_\uparrow$ is the electric field expressed by eq A2, which is produced by the free charges in the absence of the material undergoing orientational polarization, whereas P is the orientational polarization, namely, the dipole moment per unit volume of the dielectric material. In eq A3 N_w is the number of water molecules per unit surface and $\langle\mu_\uparrow\rangle$ is the mean normal component of the permanent dipole moment of the water molecules. N_w is estimated by ascribing to a water molecule the area occupied in a hexagonal lattice of lattice constant $2r_w$, i.e., $2\sqrt{3}r_w^2$: N_w is then obtained by subtracting from its maximum value, $[2\sqrt{3}r_w^2]^{-1}$, the number density of the adsorbed bromide ions times $(r_{Br}/r_w)^2$. In expressing P we have considered that the water molecules are not actually point dipoles, but have a finite size: hence, P has been smeared out over the thickness d of the adsorbed monolayer. The second term in eq A3 accounts for the effect of the water dipoles upon the extent of electron spillover. By substituting $F_\uparrow$ from eq A2 into eq A3 and neglecting the terms that do not contain α as well as the vanishingly small terms in $\exp(-\alpha d)$, we obtain

$$E_{es} = \frac{\pi}{4\alpha}\left(\frac{n^{*2}}{\alpha^2} + \sigma_M^2\right)\left(1 + \frac{1}{\epsilon_\uparrow^2}\right) + \frac{\pi n^*\sigma_M}{2\alpha^2}\left(1 - \frac{1}{\epsilon_\uparrow^2}\right) + \frac{\pi}{\epsilon_\uparrow\alpha}\left(\frac{n^*}{\alpha} - \sigma_M\right)\left(\frac{2\sigma_M}{\epsilon_\uparrow} - \frac{\langle\mu_\uparrow\rangle N_w}{d}\right) + \frac{2\pi\sigma_i}{\epsilon_\uparrow^2\alpha}\left(\frac{n^*}{\alpha} - \sigma_M\right)e^{-\alpha\beta}$$

The imaging conditions on the metal side of the monolayer are affected by the change in the surface dipole potential due to electron spillover. To estimate the latter change relative to the zero charge, we must single out the contribution $\rho_{so}(x)$ from electron spillover to the volume charge density $\rho(x)$ of eq A1. This contribution, which excludes the contribution stemming from the excess charge density σ_M, is clearly given by

$$\rho_{so}(x) = \begin{cases} n^*e^{\alpha x}/2 & \text{for } x < 0 \\ -n^*e^{-\alpha x}/2 & \text{for } x > 0 \end{cases}$$

By substituting $\rho_{so}(x)$ in the Poisson differential equation, integrating twice, and noting that $\int_{-\infty}^{+\infty}\rho_{so}(x)\,dx = 0$, the change in the surface dipole potential due to electron spillover in passing from $\sigma_M = 0$ to $\sigma_M = \sigma_M$ is given by

$$2\pi n^*(1 + 1/\epsilon_\uparrow)(1/\alpha^2 - 1/\alpha_0^2)$$

where α and α_0 are the values of the variational parameter for $\sigma_M = \sigma_M$ and $\sigma_M = 0$, respectively. To account for the effect of this change on the imaging conditions, such a change can be formally equated to the change produced by a shift of the jellium edge by an amount x_{im} following the same change in σ_M, i.e. $-4\pi\sigma_M x_{im}$. This provides the following expression for the position x_{im} of the image plane:

$$x_{im} = (n^*/2\sigma_M)(1 + 1/\epsilon_\uparrow)(1/\alpha_0^2 - 1/\alpha^2)$$

which reduces to the expression reported in ref 62 when $\epsilon_\uparrow = 1$. Note that the image plane sits in front of the jellium edge (i.e. x_{im} is >0) for all σ_M values.

The further contribution to $\bar{F}_\uparrow$ from the adsorbed water dipoles requires an estimate of the mean value $\langle\mu_\uparrow\rangle$ of the normal component of their permanent dipole moment as a function of σ_M. To this end, we will consider a sample of water molecules enclosed in a disc that is tangent to any three neighboring bromide ions arranged in the hexagonal array of lattice constant s; the radius of this disc, henceforth referred to as the "water disc", is therefore equal to $r_{wd} = s/\sqrt{3} - r_{Br}$. This sampling procedure is based on the consideration that a translation of this disc along the three axes of the array practically covers the whole surface with a modest overlapping. The horizontal component $F_\rightarrow$ of the electric field created within the water disc by the surrounding anions is estimated by assuming that the charge of these anions is smeared out uniformly on the $x = \beta$ plane, outside the disc. The effect of the uniform charge distribution of density σ_i outside the disc is equal to that of a charge density $-\sigma_i$ inside the disc. The potential that a disc of positive charge density $-\sigma_i$ and its infinite regress of images at $x = d$ and at the image plane $x = x_{im}$ create inside the disc is given by[19]

$$\phi_{disc}(R) = -\frac{4d'\sigma_i}{\pi\epsilon_{\rightarrow}}\sum_{n=1}^{\infty}\frac{a_n}{n^2}[1 - nAK_1(nA)\, I_0(nR)] \quad \text{(A4)}$$

where

$$d' \equiv d - x_{im}; \quad \beta' \equiv \beta - x_{im}; \quad R \equiv \frac{\pi r}{d'}; \quad A \equiv \frac{\pi r_{wd}}{d'};$$
$$B \equiv \frac{\pi\beta'}{d'}; \quad a_n = 1 - \cos(2nB)$$

K_1 is the Bessel function of the second kind with imaginary argument and of order 1, I_0 is the modified Bessel function of the first kind with imaginary argument and of order 0, r is the distance from the center of the water disc, and $\epsilon_\rightarrow$ is the effective distortional dielectric constant in the direction parallel to the adsorbed monolayer.

The radial component $F_\rightarrow$ of the electric field inside the water disc is given by $-d\phi_{disc}(R)/dr$. Its mean value $\bar{F}_\rightarrow$ throughout the disc is given by

$$F_\rightarrow(A) = \frac{1}{\pi r_{wd}^2}\int_0^{r_{wd}} F_\rightarrow(r)\, 2\pi r\, dr =$$
$$-\frac{8\sigma_i}{A\epsilon_{\rightarrow}}\sum_{n=1}^{\infty}[a_n K_1(nA)\int_0^A I_1(nR)R\, dR]$$

where I_1 is the modified Bessel function of the first kind with imaginary argument and of order 1. For simplicity, we will assume that both the point dipoles of the water molecules and the point charges of the bromide ions lie on the same plane $x = \beta$. Each water dipole within the water disc is considered to be subjected both to the mean horizontal field $\bar{F}_\rightarrow$ and to a mean vertical field $\bar{F}_\uparrow$; the latter is the sum of the vertical field $\bar{F}_\uparrow$ of eq A2 due to the free charges, the self-image field F_{self} of the given water dipole, and the mean field $\bar{F}_{dip}$ created by the surrounding water dipoles:

$$\bar{F}_\uparrow = \frac{4\pi\sigma_M}{\epsilon_\uparrow} + \frac{2\pi}{\epsilon_\uparrow}\left(\frac{n^*}{\alpha} - \sigma_M\right)e^{-\alpha\beta} + F_{self} + \bar{F}_{dip}$$

The mean field $\bar{F}_{dip}$ at the position of a given water dipole is estimated by assuming that the surrounding water dipoles are distributed uniformly in the adsorbed monolayer and that they have the same dipole-moment normal component $\mu_\uparrow$. $\bar{F}_{dip}$ is obtained by summing the contributions to the electric field at the "central" water dipole from the normal components of the surrounding dipoles and from their infinite images. Taking into account that the infinite images of any dipole are at distances $(2\beta' - 2nd')$ and $(2nd')$ from the center of the dipole, where n is an integer, the electric field created at the central dipole by a water dipole at a distance r and by its infinite images is given by

$$F_{dip}(r) = \frac{\mu_\uparrow}{\epsilon_{\rightarrow}}\sum_{n=-\infty}^{+\infty}\left[\frac{3(2nd')^2 - r_1^2}{r_1^5} + \frac{3(2\beta' - 2nd') - r_2^2}{r_2^5}\right] \quad \text{(A5)}$$

where $r_1 = \sqrt{(r^2+4n^2d'^2)}$ and $r_2 = \sqrt{[r^2+(2\beta'-2nd')^2]}$. In practice this summation converges for $|n| > 30$. The electric field $\bar{F}_{dip}$ is then obtained by multiplying $F_{dip}(r)$ by the number of water molecules contained in an annulus of radius r and infinitesimal thickness dr, $N_w 2\pi r\, dr$, and by integrating over distance starting from the minimum distance $2r_w$ between two water dipoles:

$$\bar{F}_{dip} = N_w\int_{2r_w}^{\infty} F_{dip}(r)2\pi r\, dr$$

In practice this integral converges for $r > 10$ Å. By considerations analogous to those yielding eq A5, the self-image electric field is given by the expression

$$F_{self} = \frac{2\mu_\uparrow}{\epsilon_\uparrow}[(2\beta')^{-3} + \sum_{\substack{n=-\infty \\ n\neq 0}}^{+\infty}(|2nd'|^{-3} + |2\beta' - 2nd'|^{-3})]$$

The mean overall electric field acting on the water dipoles has a magnitude $\bar{F} = \sqrt{(\bar{F}_\uparrow^2+\bar{F}_\rightarrow^2)}$ and is at an angle $\theta = \arccos(\bar{F}_\uparrow/\bar{F})$ with the plane of the adsorbed monolayer. The mean component $\langle\mu_\theta\rangle$ of the water dipoles along any of the infinite directions of this overall field is obtained by applying the Langevin function[63] in order to account for the effect of thermal agitation:

$$\langle\mu_\theta\rangle = \mu_w(\coth u - 1/u) \quad \text{with} \quad u = \mu_w\bar{F}/(RT)$$

whereas the mean normal component is given by $\langle\mu_\uparrow\rangle = \langle\mu_\theta\rangle\bar{F}_\uparrow/\bar{F}$. This value is continuously updated by estimating via eq A3 its effect on the extent of electron spillover, which in turn affects $\langle\mu_\uparrow\rangle$ by altering the screening effect via a shift in the position x_{im} of the image plane. This iterative procedure is repeated until convergence is achieved.

The Local Potential. To predict the shape of the adsorption isotherm, the mean value of the local potential $(-1/e)\int_0^{-e}\phi_{loc}\, dq$ during the charging process at the position of an adsorbed anion (henceforth referred to as the "central" anion) must be estimated. Three contributions to the mean local potential must be considered, namely,the contributions from the inhomogeneous electron gas, the surrounding adsorbed anions, and the surrounding water dipoles. The first contribution is obtained by substituting the charge density $\rho(x)$ of eq A1, with the exclusion of the $\delta(\beta-x)\sigma_i$ term due to the adsorbed anions, in the Poisson differential equation of electrostatics and by integrating twice; the potential difference between $x = \beta$ and $x = d$ so obtained is given by

$$\frac{4\pi\gamma\sigma_M}{\epsilon_\uparrow} + \frac{2\pi}{\alpha\epsilon_\uparrow}\left(\frac{n^*}{a} - \sigma_M\right)\exp(-\alpha\beta) \quad \text{(A6)}$$

The contribution to $(-1/e)\int_0^{-e}\phi_{loc}\,dq$ from the surrounding adsorbed anions is estimated by imagining to accumulate the partial charge q of the central anion starting from the original uniform charge distribution σ_i. This thought experiment produces around the charge q a charge-free circular hole, called the "exclusion disc",[16] such that the ratio of the charge q to the area of the disc is equal to σ_i: the disc radius r_{ex} is therefore equal to $r_{ex} = \sqrt{[q/(\pi\sigma_i)]}$. In the Guntelberg charging process the charge q is caused to increase from 0 to its maximum value $-e$, with a concomitant increase in the radius of the exclusion disc. As usual, the effect of a charge-free hole in a uniform charge distribution σ_i is identical to that of a disc of the same radius with a charge density $-\sigma_i$, together with its infinite regress of images. The mean value of the perturbation potential, $\phi_{p,a}$, due to the adsorbed anions at the center of the disc during the charging process is given by[19]

$$-\frac{1}{e}\int_0^{-e}\phi_{p,a}(q)\,dq = \frac{1}{e}\int_0^{-e}\frac{4d'\sigma_i}{\pi\epsilon_{\rightarrow}}\left[\frac{\pi^2\beta'\gamma}{d'^2} - \frac{\pi r_{ex}(q)}{d'}\sum_{n=1}^{\infty}\frac{a_n}{n}K_1\left(\frac{\pi n r_{ex}(q)}{d'}\right)\right]dq \quad \text{(A7)}$$

where $\gamma \equiv d' - \beta' = d - \beta$ and a_n is defined in eq A4. The local potential due to the surrounding anions is then given by the sum of the contributions from these anions to the mean potential difference between the iHp and the oHp and to the mean value of the perturbation potential:

$$\frac{4\pi\gamma\sigma_i}{\epsilon_{\uparrow}} - \frac{1}{e}\int_0^{-e}\phi_{p,a}(q)\,dq \quad \text{(A8)}$$

The local potential at the position of the central ion due to the surrounding water molecules can be estimated by considering the water molecules enclosed in the exclusion disc. These are subjected to the horizontal electric field E_{disc} due to the charge density σ_i outside the exclusion disc, which can be obtained by differentiating the expression for the corresponding potential[19] with respect to the distance ρ from the center of the disc:

$$E_{disc}(\rho) = -\frac{4\pi r_{ex}}{\epsilon_{\rightarrow}d'}\sigma_i\sum_{n=1}^{\infty}a_nK_1\left(\frac{\pi n r_{ex}}{d'}\right)I_1\left(\frac{\pi n\rho}{d'}\right)$$

A further contribution to the horizontal electric field stems from the partial charge q in the central ion, which is made to vary from 0 to $-e$ during the Guntelberg charging process. In practice, the almost full alignment of the water molecules of the primary solvation sheath in the direction of the central ion spreads the charge of the latter ion up to the edge of this sheath, of radius $r_{Br} + 2r_w$. The horizontal electric field created by this spread charge q and by its infinite regress of images outside the disc is given by[19]

$$E_{ion}(\rho) = \frac{4q}{\epsilon_{\rightarrow}d'(r_{Br} + 2r_w)}\sum_{n=1}^{\infty}a_nI_1\left[\frac{\pi n(r_{Br} + 2r_w)}{d'}\right]K_1\left(\frac{\pi n\rho}{d'}\right)$$

The water dipoles are subjected to the sum of these two horizonal electric fields, which are a function of the distance ρ and of the partial charge q, and to the mean vertical electric field $\bar{F}_{\uparrow}$ already considered. Their orientation is estimated once again by applying the Langevin function[63] to account for the effect of thermal agitation: this provides both the horizontal component $\mu_{||}(\rho,q)$ along the radial direction and the vertical component $\mu_{\perp}(\rho,q)$ of the water dipoles. The electric potential $\phi_{dip}(\rho,q)$ created at the position of the central ion of charge q by a water dipole at a distance ρ from this ion and by its infinite images is then given by

$$\phi_{dip}(\rho,q) = \sum_{n=-\infty}^{+\infty}\frac{\rho\mu_{||} - 2nd\mu_{\perp}}{\epsilon_{\uparrow}(\rho^2 + 4n^2d^2)^{3/2}} + \sum_{n=-\infty}^{+\infty}\frac{-\rho\mu_{||} + (2\beta - 2nd)\mu_{\perp}}{\epsilon_{\uparrow}[\rho^2 + (2\beta - 2nd)^2]^{3/2}} \quad \text{(A9)}$$

The local potential created by all the water dipoles enclosed within the exclusion disc is obtained by integrating $\phi_{dip}(\rho,q)$ first over ρ between the constant inner radius $(r_{Br} + 2r_w)$ and the radius $r_{ex}(q)$ of the exclusion disc, which is a function of q, and then over q between 0 and the final charge $-e$:

$$\frac{1}{-2\sqrt{3}r_w^2e}\int_0^{-e}dq\int_{r_{Br}+2r_w}^{r_{excl}(q)}\phi_{dip}(\rho,q)2\pi\rho\,d\rho \quad \text{(A10)}$$

Here $(2\sqrt{3}r_w^2)^{-1}$ is the number density of the water molecules within the exclusion disc. The water dipoles that are closer to the central ion have their positive end turned toward this ion, whereas, as we approach the edge of the exclusion disc, they tend to assume an opposite orientation due to the opposite electric field created by the surrounding anions. Naturally, the major contribution to the potential at the central ion is made by the dipoles that are closer to it; this gives rise to a net screening effect, albeit small, by the water dipoles.

Acknowledgment. The authors wish to thank Mr. Antonio De Luca and Mr. Francesco Gualchieri for technical assistance. The financial support of the Ministero della Pubblica Istruzione and of the Consiglio Nazionale delle Ricerche is gratefully acknowledged.

References and Notes

(1) Grahame, D. C. *J. Am. Chem. Soc.* **1958**, *80*, 4201−4210.
(2) Grahame, D. C.; Parsons, R. *J. Am. Chem. Soc.* **1961**, *83*, 1291−1296.
(3) Parry, J. M.; Parsons, R. *Trans. Faraday Soc.* **1963**, *59*, 241−256.
(4) Payne, R. *J. Phys. Chem.* **1965**, *69*, 4113−4123.
(5) Parsons, R.; Zobel, F. G. R. *J. Electroanal. Chem.* **1965**, *9*, 333−348.
(6) Dutkiewicz, E.; Parsons, R. *J. Electroanal. Chem.* **1966**, *11*, 100−110.
(7) Lawrence, J.; Parsons, R.; Payne, R. *J. Electroanal. Chem.* **1968**, *16*, 193−206.
(8) Payne, R. *Trans. Faraday Soc.* **1968**, *64*, 1638−1655.
(9) Sears, A. R.; Anson, F. C. *J. Electroanal. Chem.* **1973**, *47*, 521−531.
(10) D'Alkaine, C. V.; Gonzalez, E. R.; Parsons, R. *J. Electroanal. Chem.* **1971**, *32*, 57−68.
(11) Hills, G. J.; Reeves, R. M. *J. Electroanal. Chem.* **1973**, *42*, 355−371.
(12) Parsons, R.; Payne, R. *Z. Phys. Chem. NF* **1975**, *98*, 9−22.
(13) Ross Macdonald, J.; Barlow, C. A., Jr. *Surf. Sci.* **1966**, *4*, 381−395.
(14) Ross Macdonald, J.; Barlow, C. A., Jr. *J. Electrochem. Soc.* **1966**, *113*, 978−992.
(15) Barlow, C. A., Jr.; Ross Macdonald, J. In *Advances in Electrochemistry and Electrochemical Engineering*; Delahay, P., Tobias, C. W., Eds.; Interscience: New York, 1967; Vol. 6, pp 1−199.
(16) Levine, S.; Bell, G. M.; Calvert, D. *Can. J. Chem.* **1962**, *40*, 518−537.
(17) Levine, S.; Mingins, J.; Bell, G. M. *Can. J. Chem.* **1965**, *43*, 2834−2865.
(18) Levine, S.; Robinson, K.; Bell, G. M.; Mingins, J. *J. Electroanal. Chem.* **1972**, *38*, 253−269.
(19) Levine, S.; Robinson, K. *J. Electroanal. Chem.* **1973**, *41*, 159−177.
(20) Robinson, K.; Levine, S. *J. Electroanal. Chem.* **1973**, *47*, 395−411.

(21) Alekseev, Yu.V.; Popov, Yu. A.; Kolotyrkin, Ya. M. *Elektrokhimiya* **1976**, *12*, 907−914.
(22) Krylov, V. S.; Myamlin, V. A. *Elektrokhimiya* **1977**, *13*, 210−215.
(23) Krylov, V. S.; Kir'yanov, V. A. *Elektrokhimiya* **1977**, *13*, 1740−1743.
(24) Kuznetsov, An.; Reinhold, J.; Lorenz, W *J. Electroanal. Chem.* **1984**, *164*, 167−175.
(25) Philpott, M. R.; Glosli, J. N.; Zhu, S.-B. *Surf. Sci.* **1995**, *335*, 422−431.
(26) Frumkin, A. N.; Polianovskaya, N.; Grigoryev, N.; Bagotskaya, I. A. *Electrochim. Acta* **1965**, *10*, 793−802.
(27) Morozov, A. M.; Grigor'ev, N. B.; Bagotskaya, I. A. *Elektrokhimiya* **1966**, *2*, 1235−1239.
(28) Frumkin, A. N.; Grigor'ev, N. B.; Bagotskaya, I. A. *Elektrokhimiya* **1966**, *2*,329−333.
(29) Frumkin, A. N.; Grigor'ev, N. B. *Elektrokhimiya* **1968**, *4*, 533−535.
(30) Bagotskaya, I. A.; Morozov, A. M.; Grigor'ev, N. B. *Electrochim. Acta* **1968**, *13*, 873−879.
(31) Bagotskaya, I. A.; Potapova, E. N. *Elektrokhimiya* **1970**, *6*, 855−857.
(32) Frumkin, A. N.; Bagotskaya, I. A.; Grigor'ev, N. B. *Denki Kagaku* **1975**, *43*, 2−8; *Z. Phys. Chem. NF* **1975**, *98*, 3−7.
(33) Frumkin, A. N.; Damaskin, B; Grigor'ev, N. B.; Bagotskaya, I. A. *Electrochim. Acta* **1974**, *19*, 69−74.
(34) Trasatti, S. In *Modern Aspects of Electrochemistry*; Bockris, J. O'M., Conway, B. E., White, R. E., Eds.; Plenum: New York, 1980; Vol. 13, pp 81−206.
(35) Butler, J. N.; Meehan, M. L. *J. Phys. Chem.* **1966**, *70*, 3524−3534.
(36) Pezzatini, G.; Moncelli, M. R.; Foresti, M. L.; Pergola, F.; Guidelli, R. *J. Electroanal. Chem.* **1985**, *196*, 429−438.
(37) Horanyi, T. S.; Takacs, M. *J. Electroanal. Chem.* **1986**, *215*, 83−91.
(38) Dubova, L.; De Battisti, A.; Trasatti, S. *Electrochim. Acta* **1986**, *31*, 881−883.
(39) Foresti, M. L.; Pezzatini, G.; Monteagudo, J. C. G. *J. Electroanal. Chem.* **1990**, *295*, 251−264.
(40) Pezzatini, G.; Foresti, M. L.; Innocenti, M.; Guidelli, R. *J. Electroanal. Chem.* **1990**, *295*, 265−273.
(41) Pezzatini, G.; Moncelli, M. R.; Innocenti, M.; Guidelli, R. *J. Electroanal. Chem.* **1990**, *295*, 275−290.
(42) Pezzatini, G.; Moncelli, M. R.; Guidelli, R. *J. Electroanal. Chem.* **1991**, *301*, 227−240.
(43) Pezzatini, G.; Foresti, M. L.; Moncelli, M. R.; Guidelli, R. *J. Colloid Interface Sci.* **1991**, *146*, 452−462.
(44) Foresti, M. L.; Pezzatini, G.; Innocenti, M.; Duarte, M. Y. *J. Electroanal. Chem.* **1992**, *336*, 99−112.
(45) Innocenti, M.; Pezzatini, G.; Foresti, M. L.; Guidelli, R. *J. Electroanal. Chem.* **1993**, *349*, 113−126.
(46) Bagotskaya, I. A.; Damaskin, B. B.; Kazarinov, V. E. *Elektrokhimiya* **1995**, *31*, 471−478.
(47) Grahame, D. C.; Soderberg, B. A. *J. Chem. Phys.* **1954**, *22*, 449−460.
(48) Harned, H. S.; Crawford, C. C. *J. Am. Chem. Soc.* **1937**, *59*, 1903−1905.
(49) Davies, C. W. *J. Chem. Soc.* **1938**, 2093−2098.
(50) Bange, K.; Straehler, B.; Sass, J. K.; Parsons, R. *J. Electroanal. Chem.* **1987**, *229*, 87−98.
(51) Schmickler, W.; Guidelli, R. *J. Electroanal. Chem.* **1987**, *235*, 387−392.
(52) Schmickler, W. *J. Electroanal. Chem.* **1988**, *249*, 25−33.
(53) Foresti, M. L.; Aloisi, G.; Innocenti, M.; Kobayashi, H.; Guidelli, R. *Surf. Sci.* **1995**, *335*, 241−251.
(54) Schultze, J. W.; Vetter, K. J. *J. Electroanal. Chem.* **1973**, *44*, 63−81.
(55) De Levie, R. *J. Electrochem. Soc.* **1971**, *118*, 184C−192C.
(56) Carla', M.; Aloisi, G.; Foresti, M. L.; Guidelli, R. *J. Electroanal. Chem.* **1986**, *197*, 123−141.
(57) Guidelli, R. In *Adsorption of Molecules at Metal Electrodes*, Lipkowski, J., Ross, P. N., Eds.; VCH: Cambridge, U.K., 1992; pp 1−76.
(58) Guidelli, R. *J. Chem. Phys.* **1990**, *92*, 6152−6160.
(59) Partenskii, M.; Smorodinskii, Ya. *Sov. Phys. Solid State* **1974**, *16*, 423−429.
(60) Smith, J. R. *Phys. Rev.* **1969**, *181*, 522−529.
(61) Böttcher, C. J. *Theory of Electric Polarization*; Elsevier: Amsterdam, 1973; Vol. 1, pp 103−109.
(62) Kornyshev, A. A. *Electrochim. Acta* **1989**, *34*, 1829−1847.
(63) Ref 61, pp 161−165.